http://sure.sunderland.ac.uk/policies.html or alternatively contact sure@sunderland.ac.uk.

Brain Research Bulletin 163 (2020) 72–83

Long-Term Effects of Experimental Carotid Stenosis on Hippocampal Infarct Pathology, Neurons and Glia and Amelioration by Environmental Enrichment

William Stevenson1; Yoshiki Hase1; Elle Wilson1; Annabel Hollins1; Mai Hase1, Abdel Ennaceur2, Lucy Craggs1, Masafumi Ihara3, Karen Horsburgh4, and Raj N Kalaria1

1 Neurovascular Research Group, Translational and Clinical Research Institute, Newcastle University, Newcastle upon Tyne, UK
2 Department of Pharmacy, Sunderland Pharmacy School, The University of Sunderland, Sunderland, UK
3 Department of Neurology, National Cerebral and Cardiovascular Centre, Osaka, Japan
4 Centre for Discovery Brain Sciences, The University of Edinburgh, Edinburgh, UK Running headline: Environmental enrichment on hippocampal pathology

Corresponding author:
Professor Raj N. Kalaria
Translational and Clinical Research Institute, Newcastle University, Campus for Ageing and Vitality, Newcastle upon Tyne, NE4 5PL, United Kingdom
Tel: +44-(0)191-208-1352
e-mail: raj.kalaria@newcastle.ac.uk

PII: S0361-9230(20)30571-2
DOI: https://doi.org/10.1016/j.brainresbull.2020.07.014
Reference: BRB 9967
To appear in: Brain Research Bulletin
Received Date: 14 April 2020
Revised Date: 3 July 2020
Accepted Date: 15 July 2020

Highlights

- Long-term carotid stenosis in mice caused hippocampal infarcts and neuron loss
- Long-term carotid stenosis (BCAS) also induced reactive astrocytes and microglia
- Environmental Enrichment (EE) attenuated BCAS-induced infarcts and cellular changes
- Cognitive decline (working memory) after long-term BCAS was also ameliorated by EE
- EE would be an effective interventional strategy for vascular cognitive impairment

Abstract

Hippocampal atrophy and pathology are common in ageing-related disorders and associated with cognitive impairment and dementia. We explored whether environmental enrichment (EE) ameliorated the pathological sequelae in the hippocampus subsequent to chronic cerebral hypoperfusion induced by bilateral common carotid artery stenosis (BCAS). Seventy-four male C57BL/6 J mice underwent BCAS or sham surgery. One-week after surgery, mice were exposed to three different degrees of EE; either standard housing conditions (std), limited 3-h exposure to EE per day (3 h) or full-time exposure to EE (full) for 3 months. Four months after surgery, the hippocampus was examined for the extent of vascular brain injury and neuronal and glial changes. Results showed that long-term BCAS induced strokes, most often in CA1 subfield, reduced 40–50 % CA1 neurons ($P<0.01$) and increased microglia/macrophage in CA1-CA3 subfields ($P<0.02$). Remarkably, both 3 h and full-time EE regimes attenuated hippocampal neuronal death and repressed recurrent strokes with complete prevention of larger infarcts in mice on full-time EE ($P<0.01$). Full-time EE also reduced astrocytic clasmatodendrosis and microglial/macrophage activation in all CA subfields. Our results suggest that exposure to EE differentially reduces long-term hypoperfusive hippocampal damage. The implementation of even limited EE may be beneficial for patients diagnosed with vascular cognitive impairment.

Keywords: Animal model; chronic cerebral hypoperfusion; environmental enrichment; hippocampus; vascular cognitive impairment; vascular dementia

1. Introduction

Vascular dementia (VaD) is the second most common form of dementia, precipitated by accumulative cerebrovascular lesions (Kalaria, 2016). Chronic cerebral hypoperfusion has been suggested to be an important substrate of subcortical ischaemic vascular dementia (SIVD), the most common subtype of VaD (Hachinski et al., 2006; Roman et al., 2002). SIVD is characterized by white matter changes and lacunar infarctions in which cerebral blood flow (CBF) is decreased over an extended period of time because of small vessel changes (Pantoni, 2010). This can promote white matter (WM) changes (Roman et al., 2002), frontal hypo-metabolism (Tullberg et al., 2004) and the cognitive impairment (de Groot et al., 2000) seen in dementia as well as vascular cognitive impairment (VCI).

There is considerable evidence that the pathological changes in the hippocampus are central to the development of cognitive impairment in ageing and dementia caused by both cerebrovascular lesions and neurodegenerative disease (Grysiewicz and Gorelick, 2012). Hippocampal atrophy is also associated with cerebrovascular disease, including ischaemic vascular dementia, ageing-related SVD, hereditary SVD and post-stroke dementia (Zarow et al., 2005). Hippocampal atrophy further occurs in subjects with subtle memory impairments and in mild cognitive impairment (MCI) (Grundman et al., 2003), and increases risk of dementia in cognitively normal elderly subjects (den Heijer et al., 2006).

The bilateral carotid artery stenosis (BCAS) in mice has been widely used in recent times to simulate the effects of SVD and study the sequelae of cerebral hypoperfusion. As one of the most reliable brain noninvasive rodent models, it has been used to evaluate the pathophysiology of VaD (Bink et al., 2013; Holland et al., 2015; Ihara and Tomimoto, 2011; Madigan et al., 2016). It replicates several pathological hallmarks of SIVD including impaired blood-brain barrier integrity, diffuse lesions in the deep white matter and internal border zones and neuroinflammation. Chronic neurodegenerative diseases are accelerated by inflammatory responses with the involvement of both microglial/macrophage and astrocytic proliferation and activation (Gomez-Nicola et al., 2013). Following neuronal or glial damage, inflammatory response, characterised by microglial/macrophage activation, has been demonstrated as having both beneficial and detrimental effects in various neurological diseases, e.g. stroke and Alzheimer's disease (Rawji et al., 2016). However, chronic over-activation of microglia may cause progressive neurotoxic effects in the brain (Wu et al., 2014).

Environmental enrichment (EE) has been proposed as a prevention strategy to improve cognitive function in humans and possibly reverse WM and neuronal damage (Hase et al., 2018). Evidence shows that physical and cognitive stimulations, which are incorporated in EE and physical exercise training, could enhance synaptic plasticity and attenuate cognitive deficits in rodents and man (Bayat et al., 2015; Cechetti et al., 2012; Fischer, 2016; Sun et al., 2010). These studies showed that EE increased brain plasticity, enhanced neurogenesis, and increased synaptogenesis as well as preserved motor and cognitive function. Although several previous studies reported the beneficial effects of EE in rodents and man, few studies explored the protective effects of differing degrees of EE in VaD. Here, we investigated the effects of different degrees of EE on the pathological sequelae in mice subjected to BCAS, with the aim of assessing stroke pathology and morphological changes specifically in the hippocampus (Hase et al., 2018; Hase et al., 2019) and cognitive function as they relate to VCI and VaD.

2. Materials and Methods

2.1. Animals and surgical procedures

The experimental paradigm of the study is depicted in Fig. 1. Male C57BL/6 J mice (2.1 months old, 23.1 − 25.3 g) were purchased from the Jackson Laboratory, USA. The mice

were housed within a 12-h day and 12-h night cycle (6 am–6 pm, day; 6 pm–6 am, night) and were given access to food and water ad libitum. After 1-week acclimatisation, a total of 74 mice were randomly assigned for either bilateral common carotid artery stenosis (BCAS, n = 41) or sham (n = 33) surgery. BCAS surgery was performed as previously described (Hase et al., 2018; Shibata et al., 2004). Briefly, mice were anaesthetised by 1.5 % isoflurane in oxygen and air. A middle neck incision was made, the common carotid arteries (CCAs) were then exposed and isolated from the vagus nerves. Microcoils, (internal lumen - 0.18 mm (Sawane Spring, Japan)), were applied to both CCAs. Sham animals were exposed to the same operative procedures as BCAS mice, except for the application of microcoils. Body temperature was monitored and maintained between 36.5 and 37.5 °C with the aid of a feedback warming pad and a blanket during the operative procedure. Animals were appropriately identified with coded numbers. All of the experiments and data analyses were performed under investigator-blinded conditions. Animals dying during the experimental period and before the planned euthanisation at 4 months after surgery were excluded from further analyses. All procedures were pre-approved by the Home Office, London, UK based upon ASPA: The Animals (Scientific Procedures) Act 1986, UK and performed in accordance with the guidelines stipulated by the ethical committee of Newcastle University and adhering to ARRIVE guidelines.

2.2. Environmental enrichment (EE) paradigm and animal groups

One week after surgery, mice were randomly assigned to six subgroups: Sham-std, sham-operated mice with standard housing; Sham-3 h, sham-operated mice with limited exposure to EE; Sham-full, sham operated mice with full-time exposure to EE; BCAS-std, BCAS operated mice with standard housing; BCAS-3 h, BCAS operated mice with limited exposure to EE and BCAS-full, BCAS operated mice with full-time exposure to EE. Standard housing denotes a normal housing condition, which incorporated a paper house and shredded tissue. EE cages had extra toys in addition to the standard housing, e.g. running wheels, hanging chains, igloos and a paper tunnel. Limited exposure to EE was performed as described previously (Lazarov et al., 2005). Briefly, for the first month, mice were transferred to the EE cages for 3 h every day in the morning from 9 a.m. to 12 pm. From second month to end of third month, mice experienced EE cages for 3 h, 3 days per week. Fulltime exposure to EE group experienced an EE environment every day for 24 h over the entire 3 months. In this study, the experimental animals (survivors) were divided into six groups with the following numbers: Sham-std, n = 11; Sham-3 h, n = 11; Sham-full, n = 11; BCAS-std, n = 13; BCAS-3 h, n = 10; BCAS-full, n = 12.

2.3. Histopathological analysis

Mice were anaesthetised by intraperitoneal injection of sodium pentobarbital (50 mg/kg) and perfused transcardially at 20 ml/min with 0.01 M phosphate-buffered saline (PBS), pH 7.4. Brains were removed and divided into two hemispheres. The right or left hemisphere of each brain was randomly assigned for histological analysis and post fixed in 4% paraformaldehyde (PFA) in 0.01 M PBS (pH 7.4) for 48 h. Each hemisphere was cut into five blocks at different coronal levels after fixation: Block OB, coronal level of olfactory bulb (OB); Block 1, coronal level of bregma +0.5 mm; Block 2, coronal level of bregma −1.0 mm; Block 3, coronal level of bregma − 2.0 mm; Block 4, level of cerebellum and brain stem. Each sub-dissected block was dehydrated and embedded in paraffin to produce 5-μm thick sections (n = 2–4) for histological staining and analysis.

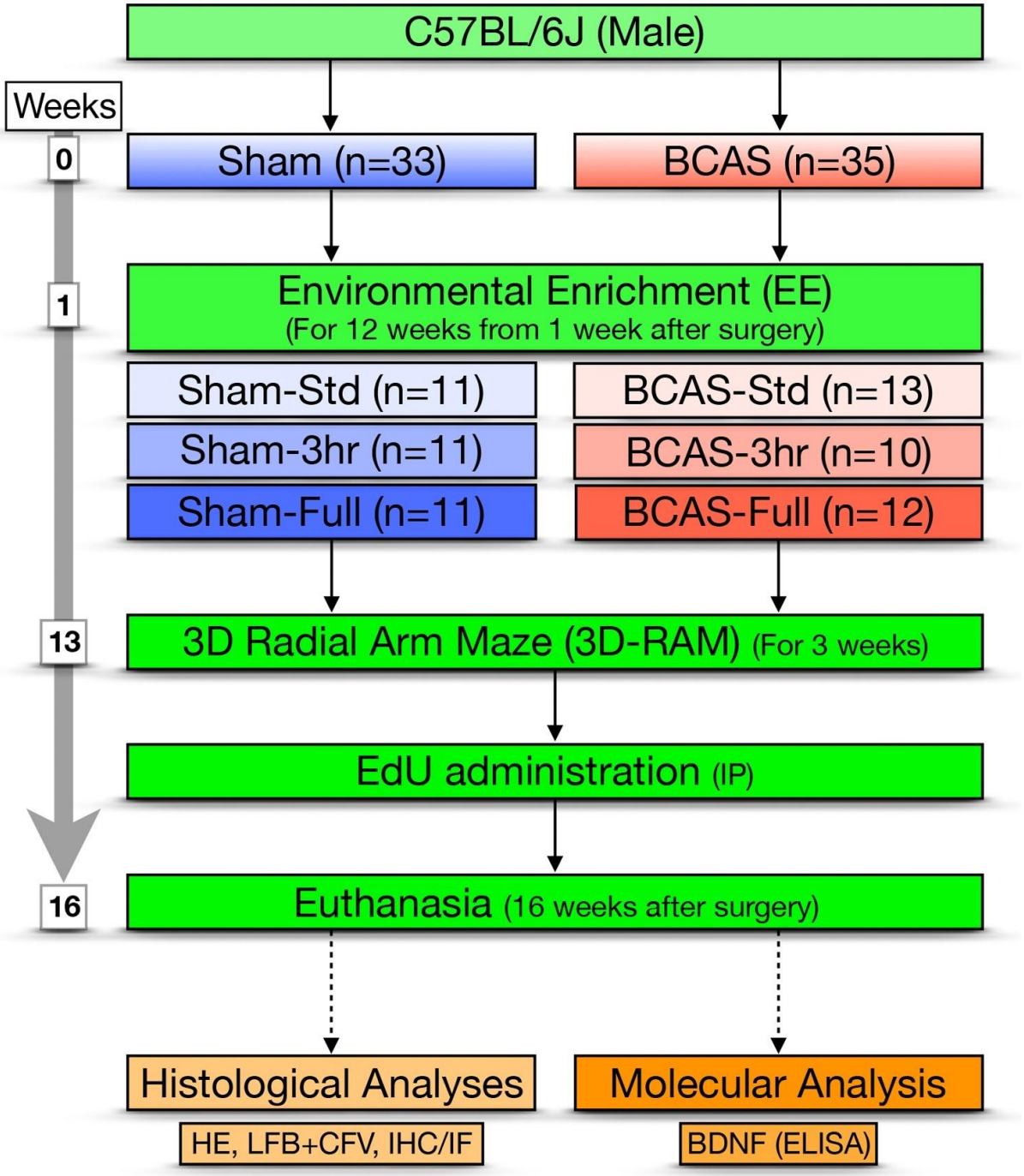

Fig. 1. Experimental Protocol and animal groups in this study.
BCAS, Bilateral Common Carotid Artery Stenosis; EE, Environmental Enrichment; Std, standard housing; 3 h, Limited EE (Three hours per day); Full, Full-time EE (24 h a day); RAM, radial arm maze; EdU, 5-ethynyl-2'-deoxyuridine; IP, Intraperitoneal injection; HE, Haematoxylin and Eosin; LFB + CFV, Luxol Fast Blue and Cresyl Fast Violet; IHC/IF, Immunohistochemistry/ Immunofluorescence; BDNF, Brain-derived neurotrophic factor; ELISA, Enzyme-linked immunosorbent assay.

2.4. Incidence, distribution and volume of strokes

H&E and Klüver–Barrera stained serial sections obtained from the block 3 (coronal level of -2.0 mm from the bregma) were used to determine stroke pathology in mice hippocampus. Images were captured using a bright field microscope (Leitz DIALUX 20; Leica) with 5×, 10× and 20× objective lenses coupled to a Lumenera infinity digital

camera (Lumenera Corporation). The presence of ischaemic or haemorrhagic infarcts and microhaemorrhages was recorded in each mouse. Incidence of hippocampal strokes in each group was calculated. First, we determined the number of infarcts in the hippocampal formation was counted in each mouse, and then the average number of strokes was calculated for each group. We subsequently determined the volumes, location and percentage of these lesions. To assess stroke volumes in each mouse, the damaged area was traced using ImageJ software (National Institutes of Health, Bethesda, MD, USA). Stroke area (mm2) was calculated and multiplied by the thickness (mm) of each block.

2.5. Histological and immunohistochemical analysis

At the outset, we were careful to assess all neuronal and glial cell counts in regions of interest generally devoid of any obvious infarction. Histological analysis for the neuronal counts was performed by staining with H&E according to standard protocols. For NeuN immunohistochemistry sections were treated for antigen retrieval by boiling in Tris sodium citrate buffer (pH 6) and subsequently quenched in 3% hydrogen peroxide (H2O2) in PBS. Blocking was performed using 10 % normal goat serum (NGS) in 0.05 M PBS. Sections were incubated with primary rabbit anti-NeuN antibody (ABN78; diluted 1:500 in PBS, Millipore, Burlington, MA, USA), washed in PBS, and exposed to rabbit secondary antibody (diluted 1:200 in PBS, Vector Laboratories, Burlingame, CA, USA). Finally, samples were developed using avidin-biotin complex (ABC) (PK-6101, Vector Laboratories) and visualised with the chromogen 3,3′-diaminobenzidine (DAB).

For the glial staining, each section was microwaved for 11 min in 0.01 M citrate buffer, and then left for 30 min in 3% hydrogen peroxide (H2O2), followed by blocking, with 1:67 normal goat serum. Following that, the sections were treated with either anti-glial fibrillary acid protein (anti-GFAP) antibody (1:2000, DAKO) for astrocytes or ionised calcium-binding adaptor protein-1 (Iba-1) (1:200, Wako, Osaka, Japan) for microglia/macrophage. The slides were incubated overnight at 4 °C. Secondary antibody incubation with biotinylated anti-IgG (1:200, Vector Laboratories) and detected using ABC Kit (Vector Laboratories). For visualisation, the sections were submerged in DAB and a haematoxylin counterstain was carried out for staining of cell nuclei. Using frozen brain samples, levels of hippocampal BDNF were quantified by the Total BDNF Quantikine ELISA Kit (DBNT00, R&D Systems, MN, USA), according to manufacturer's instructions.

2.6. Hippocampal cell counts

Images of each hippocampal subfield were captured using a Zeiss Axioplan2 bright field microscope with a PLAN-Neofluar ZEISS 10x objective lens accompanied by an Infinity Capture 2 camera running on Infinity Capture (Lumerera Corporation) imaging software. For each tissue section, two images of the CA1 (CA1-1-CA1-2) were taken along with one image of the CA2-3 and CA4. The number of hippocampal neurons was determined by manually counting neurons in each region in individual images, with the assessor blinded to experimental groups. Due to the high cell density of the dentate gyrus (DG), each granule cell morphology was difficult to determine, thus precluding quantitative analysis of this region. Neuronal counts were thus performed in the CA1, CA2-3 and CA4. The average neuronal count for each hippocampal subfield was averaged from the counts of three different coronal levels of the hippocampus, from anterior to posterior. Overall counts were also calculated for each case, defined as the sum of neurons in the CA1, CA2-3 and CA4 subregions.

GFAP-positive cells and Iba-1-positive cells within each subregion of the hippocampus were manually counted from images taken with a bright field microscope (Zeiss

Axioplan2) with a 20x objective lens (PLAN-Neofluar ZEISS). Each subfield of the hippocampus was traced to determine the area (mm2) of each subregion (CA 1-4) using ImageJ software. Numerical density of GFAP-positive cells and Iba-1-positive cells were calculated (/mm2). GFAP-positive clasmatodendrocyte was morphologically defined as their loss of processes and swollen round cell body (Chen et al., 2016). Iba-1-positive microglia/macrophage was categorized into Ramified (less than 7μm in size of the cell body), Primed (the size of the cell body exceeding 7μm) and Activated (cell body size exceeding 10μm) (Hase et al., 2017).

2.7. EdU staining and quantification

The identification of proliferating cells in the dentate gyrus was performed using 5-ethynyl-2′-deoxyuridine (EdU). Mice were injected intraperitoneally with 25 mg/kg EdU dissolved in sterile PBS (5 mg/ mL) and perfused 24 h later. Tissue processing was performed as previously described. Staining was employed using a Click-iT™ Plus Alexa Fluor™ 488 Picolyl Azide Toolkit (Thermo Fisher Scientific, C10641) following the manufacturer's instructions. EdU positive (EdU+) cells were counted manually in the entire DG using an EVOS FL Color (Life Technologies) microscope with a 10x objective lens. The average number of EdU + cells was then determined for each experimental group. We also verified proliferating cells by immunostaining with antibodies to Ki67 (1:300 dilution, ab15580, Abcam, Cambridge, UK), most frequently used as a proliferating cell marker.

2.8. Working memory assessment using an innovative three-dimensional nine-arm radial maze

Cognitive function was assessed in each mouse from 3 months post BCAS surgery during a period of 3 weeks, using an innovative three dimensional (3D) nine-arm radial maze (3D-RAM) (Ennaceur et al., 2008). This was a modified version of the conventional eight-arm radial maze. Behavioural tests were performed in a dimly lit behavioural testing room. The 3D maze (grey PVC, 5 mm thick) consisted of nine arms connected to bridges (slope part) radiating from a central platform. Each arm (35 cm × 11.2 cm) was attached to a bridge (slope part at 40°, 15.2 cm × 11.2 cm). The surface of the bridge was made of metal mesh, which enabled mice to maintain grip. A small transparent wall panel (9 cm × 6 cm) was randomly placed at each entrance of a bridge in order to narrow entry, which avoids a continuous sequential entry from one bridge to the next. In order to enter each arm, mice paced in the centre platform and needed to cross a bridge (elevated ramp) (Ennaceur et al., 2008). At the end of each arm, a small pellet (Dustless Precision Pellets® Rodent, Purified, Bio Serv, USA) was placed in order to entice food-restricted mice to enter the arm. Different colours/ shapes of pictures were placed vertically at the end of each arm as visual cues, enabling mice to distinguish individual arms. The maze was placed at the centre of a behavioural test room affixed during the entire testing period. All of the sessions for each mouse were streamed and recorded using a camcorder (LEGRIA HF R56, Canon), suspended directly over the maze, via a Wi-Fi network to an iPad (Apple Inc., USA), which was sited outside the behavioural test room. A day before the first session, each mouse was weighed to ascertain body weight and food deprivation was induced to achieve 10 % reduction in their body weight. Mice were weighed immediately prior to each testing session to ensure their BW was maintained at 90 % of baseline level. Mice were randomly tested for 3 weeks on consecutive days without prior habituation to the maze (Ennaceur, 2011; Ennaceur et al., 2011). Mice placed into a transparent plastic beaker (7 cm diameter, 18.5 cm height) were gently introduced on the central platform at the start of each session. The session was terminated when each mouse completed nine-arm entries or when 10 min had elapsed. After each session, the mouse was allowed to return to the central platform before

removing it from the maze in a similarly gentle manner. Between each session, the maze was cleaned with hypochlorous acid-soaked tissue followed by distilled water to remove any trace smells left by urine or faeces. The number of arm entries before first repeat (NABFR) was recorded in each session. The number of arm entries before first repeat in every consecutive 10 sessions and overall, 20 sessions were averaged.

2.9. Statistical analysis

Statistical analysis was conducted using SPSS (version 22.0). All data are presented as the mean ±SEM. Prior to performing statistical comparisons, all data was tested for normality using the Shapiro-Wilk's test. Parametric data was assessed using a one-way ANOVA followed by Tukey post-hoc analysis. For non-parametric data, multi-group comparisons were carried out using the Kruskal-Wallis test and post hoc comparisons were performed using the Mann-Whitney U test, Correlation analyses were performed using Pearson's r or Spearman's rho where applicable. All differences were considered significant at the P=<0.05 alpha level.

3. Results

3.1. Survival rate of animals

All sham-operated mice (n = 33) survived until 4 months after surgery. As we have reported previously (Hase et al., 2018; Hase et al., 2019), survival rate of the BCAS mice was 85.4 % (35 of original 41 mice) at 4 months after surgery. Survival rates of the BCAS subgroups were as follows: BCAS-std 92.9 % (13 of 14), BCAS-3 h 91.0 % (10 of 11); BCAS-full 75 % (12 of 16). Causes of deaths were: cerebral haemorrhage (n = 1), severe enterocolitis (n = 1), kidney anomaly (n = 1) and acute renal failure due to dehydration (n = 3). The final number of survivors in each group was Sham-std, n = 11; Sham-3 h, n = 11; Sham-full, n = 11; BCAS-std, n = 13, BCAS-3 h, n = 10; BCAS-full, n = 12. Tissues from all the surviving mice were used for each of the assays.

3.2. Limited versus full-time exposure to EE reduces neuronal loss

Fig. 2a shows representative images of sections stained with HE (A–F) and for NeuN (G–L) in each group. The loss of CA1 neurons is evident in BCAS std in both HE (D) and NeuN (J) stained sections. Neuronal loss in the CA1 region caused by BCAS was ameliorated by both limited and full-time EE, with full-time EE being a more effective regime in preventing neuronal loss whether revealed by HE (P<0.01) or NeuN (P<0.05) (Fig. 2b,e) and nearly close to levels seen in the sham cohorts. Differences were also noted in the overall neuronal numbers between the two experimental groups (P<0.01). However, no significant differences were evident in the CA2−3 and CA4 neuronal counts between BCAS and sham animals (Fig. 2c–d, f–g). Correlation analysis between NeuN positive neurons and HE stained neurons showed strong positive correlations between the markers in the entire CA 1–4 (Pearson's r= 0.72, P =0.001) and CA1 subregion (Pearson's r = 0.94, P = 0.005) (Fig. 2h, j).

Brain Research Bulletin 163 (2020) 72–83

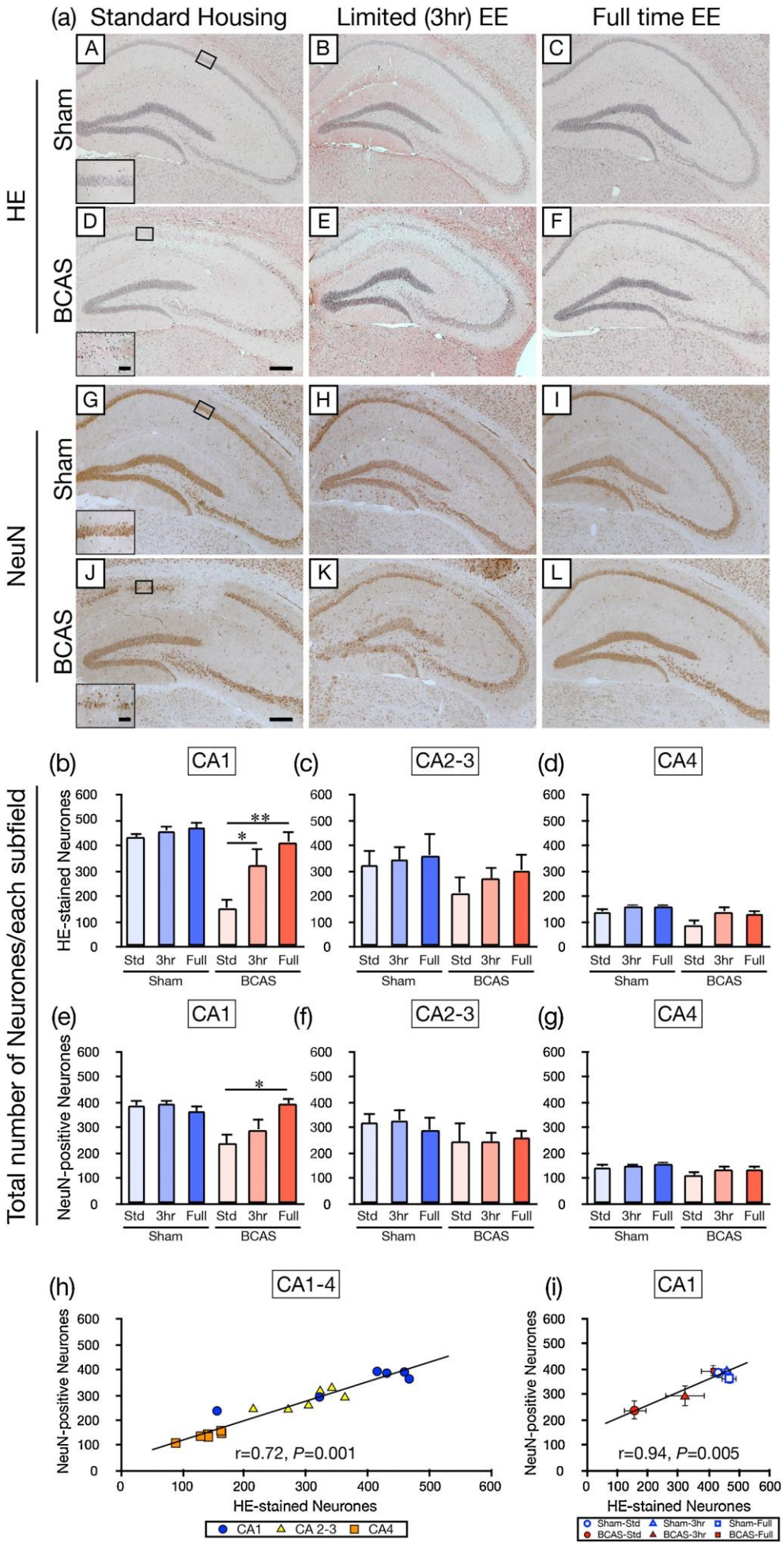

Fig. 2. Total number of Neurons in the Hippocampus after long-term bilateral common carotid artery stenosis (BCAS).
a(A–L), Representative images of Hippocampus stained with Haematoxylin and Eosin (HE) (A–F) and NeuN (G–L) in each group. a(A and G), Sham-Std; a(B and H), Sham-3 h; a(C and I), Sham-Full; a(D and J), BCAS-Std; a(E and K), BCAS- 3 h; a(F and L), BCAS-Full. a(A, D, G and J), Insets showing normal appearing CA1 neurons in Sham (a(A and G)) and CA1 neuronal loss observed in BCAS group (a(D and J)). Scale bar = 200 µm; Scale bar in insets = 50 µm. b–g, Histograms showing total number of neurons analysed by HE- (b–d) and NeuN-(e–g) stained sections in CA1 (b and e), CA2−3 (c and f) and CA4 (d and g) subfields of the Hippocampus. NeuN data obtained from two different coronal levels of sections. b, Total number of HE-stained neurons in CA1 were reduced in BCAS-Std and EE effectively restored neuronal loss (*P<0.05 and **P<0.01 respectively). e, Total number of NeuN-positive neurons in CA1 were also reduced in BCAS-Std and EE preserved CA1 neurons after long-term BCAS (*P<0.05). h and i, Graphs showing correlations between HE-stained and NeuN-positive neurons in the entire CA1–4 (h) and CA1 subfield (i). Strong positive correlations were observed between those two markers in both the entire CA 1–4 (Pearson's r = 0.72, P = 0.001) and CA1 subregions (Pearson's r=0.94, P = 0.005).

3.3. EE prevents stroke pathology

BCAS Std mice exhibited a range of infarcts in the hippocampal formation after BCAS for a duration of 4 months (Fig. 3). Incidence of strokes in the hippocampus was the highest in BCAS-std (31 %), followed by BCAS-3 h (30 %) and BCAS-full (25 %) groups, whereas none of Sham animals exhibited stroke pathologies. Average number of strokes in the hippocampus was also high in BCAS-std (2.3)>BCAS-3 h (1.7)>BCAS-full (1.3). Remarkably, average infarct volumes were attenuated by EE. For instance, stroke volume in the BCAS-full group compared to BCAS-std was significantly smaller (P = 0.008) with a similar but not significant trend observed between BCAS-full and BCAS- 3 h (P = 0.08) (Fig. 3b). Analysis of infarct sizes across the three BCAS groups showed complete reduction of the larger infarcts (> 0.1 mm3) in the BCAS-full mice compared to 33.3 % and 40.0 % for BCAS-std and BCAS-3 h, respectively (Fig. 3c). Similarly, the smallest infarct size (< 0.03 mm3) was identified least in the BCAS-std group with 11.1 %, with levels increasing in the enriched groups up to 66.7 % in the BCASfull group. These results suggest that EE importantly reduces severity of hippocampal infarcts. BCAS induced varied distribution of the location of infarcts with full-time EE resulting in no infarcts in the dentate gyrus (Fig. 3d). Infarcts across the three groups were most common in the CA1 region, followed by CA2−3 and CA4. Moreover, number of CA1 neurons were negatively correlated with total hippocampal stroke volumes (Spearman's rho= -0.57, P = 0.000).

Brain Research Bulletin 163 (2020) 72–83

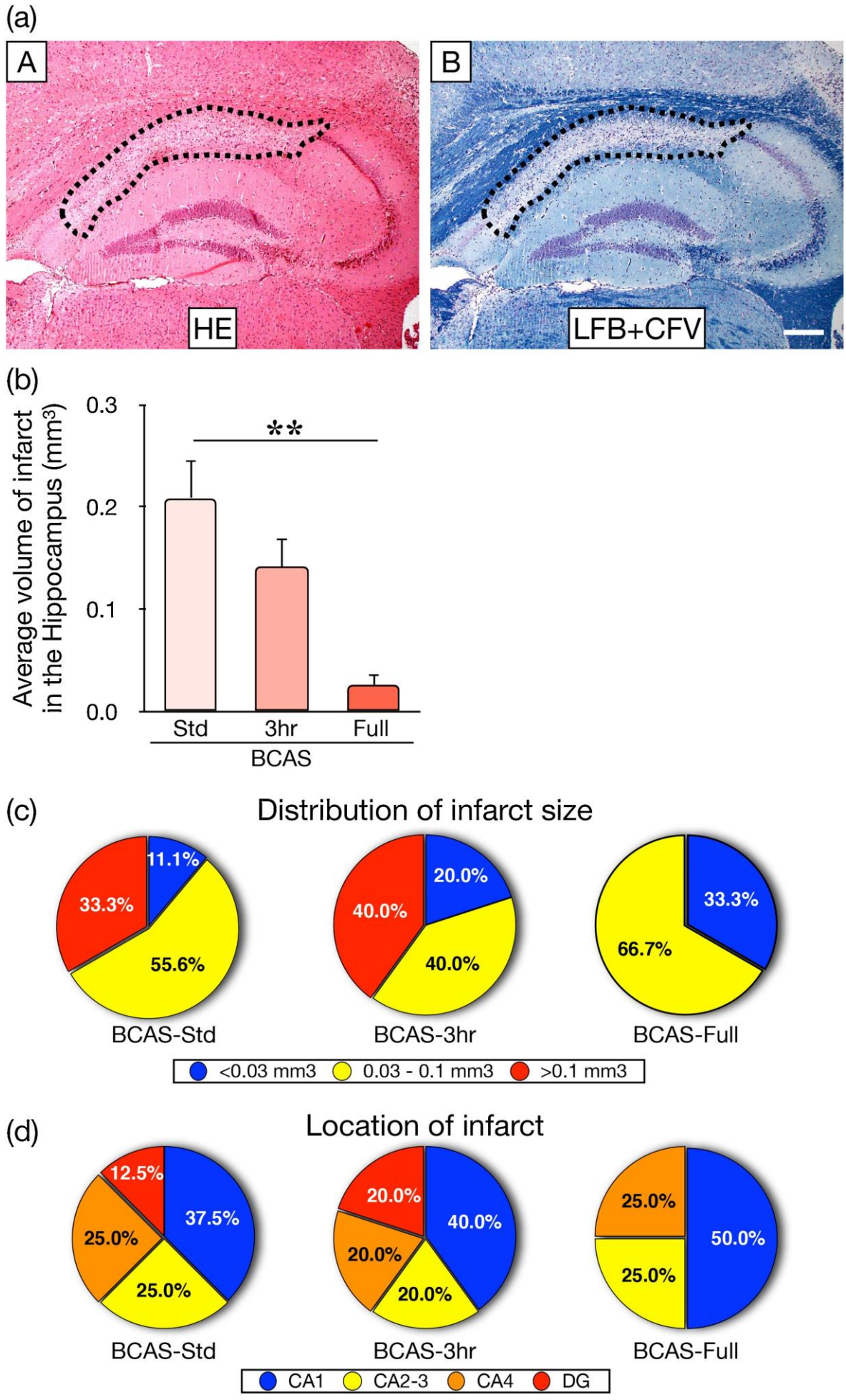

Fig. 3. Stroke Pathology in the Hippocampus induced by long-term bilateral common carotid artery stenosis (BCAS).

a(A–B), Representative images of ischaemic stroke lesions in the Hippocampus stained with HE (A) and LFB +CFV (B) after long-term BCAS. The infarct region detected in the CA1 field is delineated by the area within the dotted lines. b, Histogram showing total volume of infarcts in the Hippocampus in each BCAS subgroup. EE effectively reduced stroke volume after long-term BCAS (**P<0.01; P<0.10 BCAS-Std vs BCAS- 3 h). No infarcts were detected in Sham groups. c and d, Pie charts showing distribution of infarct size (c) and location of infarct (d) in BCAS subgroups. c, BCASStd tended to show larger infarcts whereas BCAS plus EE groups exhibited smaller infarcts. d, Majority of infarcts were observed in CA1 region across all BCAS subgroups. Dentate Gyrus was spared in BCAS-Full group. a, Scale bar = 100 µm.

3.4. Full time EE reduces astrogliosis

Representative images (Fig. 4a) of GFAP-stained hippocampal sections show increased levels of astrogliosis are evident in the BCAS-std and BCAS-3 h groups with increased astrocyte proliferation as well as a loss of astrocyte processes and cell body hypertrophy. BCAS resulted in increased density of GFAP-positive cells, in terms of the total astrocytic response (Fig. 4b–d) and of clasmatodendrocytes alone (Fig. 4e–g) in all subfields. A significant reduction in total GFAP-positive cell density was evident in the BCAS-full mice compared to BCAS-std (all P<0.001), with the CA1 region also showing a clear reduction in BCAS-3 h against BCAS-std (P=0.015). Similar results were observed between BCAS-full and BCAS-std in clasmatodendrocyte density (all p<0.001), with differences between BCAS-3 h and BCAS-std seen in all subfields (CA1: P = 0.008; CA2−3: P = 0.005 and CA4: P = 0.005) (Fig. 4e–g). EE resulted in a reduction of clasmatodendrocytes in all subfields, with full time enrichment again showing the most effect (all P<0.001 vs BCASstd), although there were also significant decreases in all subfields with limited enrichment (CA1: P=0.026; CA2−3: P=0.001 and CA4: P= 0.005) (Fig. 4h–j).

Brain Research Bulletin 163 (2020) 72–83

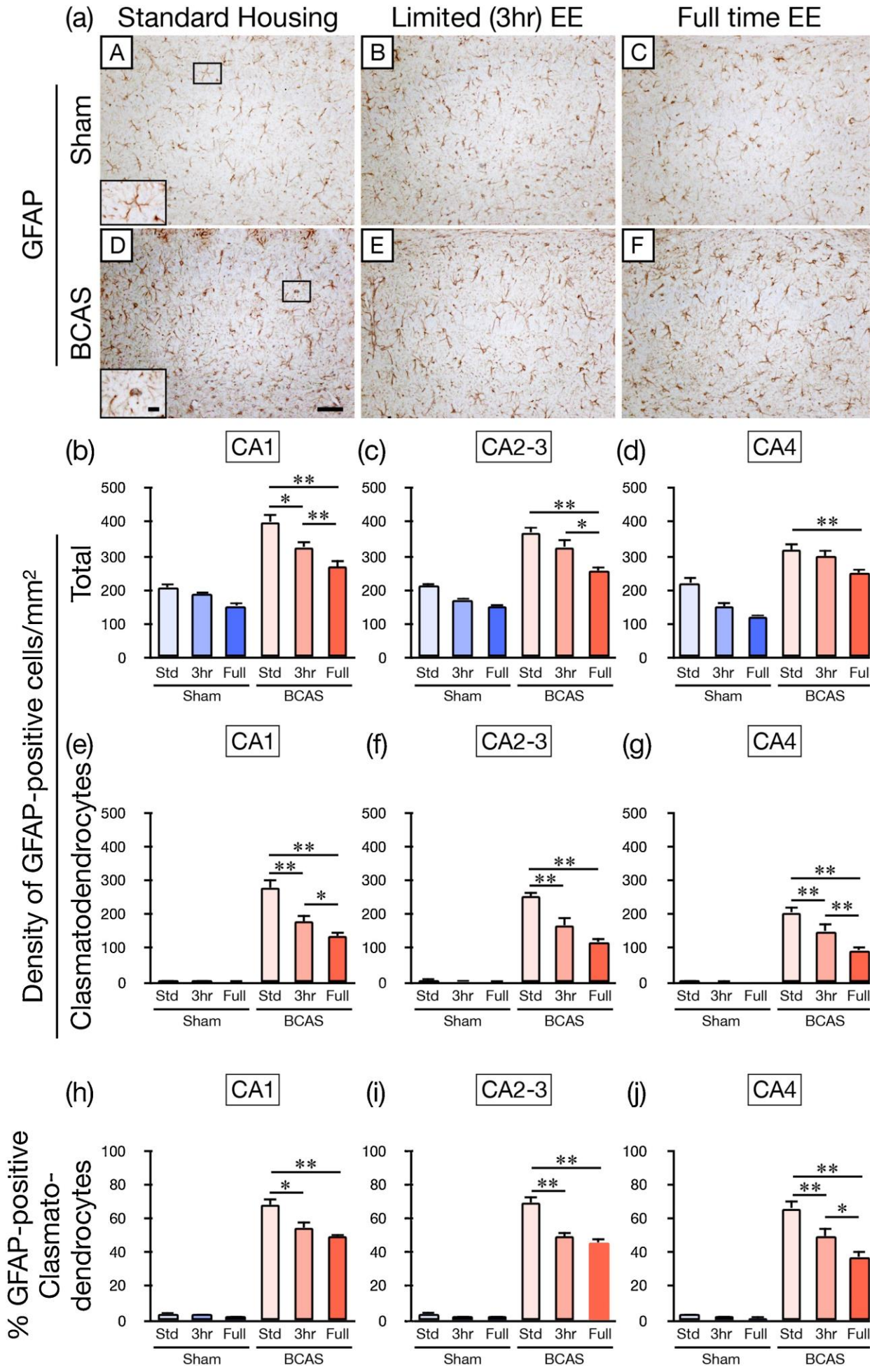

Fig. 4. Assessment of astrogliosis and clasmatodendrosis in theμ Hippocampus induced by long-term bilateral common carotid artery stenosis (BCAS).
a(A–F), Representative images of Hippocampus stained with Grial fibrillary acid protein (GFAP), a marker of astrocytes, in each group. a(A), Sham-Std; a(B), Sham-3 h; a(C), Sham-Full; a(D), BCAS-Std; a(E), BCAS-3 h; a(F), BCAS-Full. a(A and D), Insets showing a normal GFAP-positive astrocyte in Sham (a(A)) and a clasmatodendrocyte observed in BCAS group (a(D)). Scale bar=50 μm; Scale bar in insets =10 μm. b–j, Histograms showing density of total GFAP-positive cells (b–d), GFAP-positive clasmatodendrocytes (e–g) and % GFAP-positive clasmatodendrocytes (h–j) in CA1 (b, e and h), CA2−3 (c, f and i) and CA4 (d, g and j) subfields of the Hippocampus. b–g, Density of total GFAP-positive cells (astrogliosis) (b–d) and clasmatodendrocytes (clasmatodendrosis) (e–g) were increased in all subregions of Hippocampus in BCAS-Std group. EE effectively attenuated astrogliosis in all subfields (CA1 (b and e), CA2−3 (c and f) and CA4 (d and g)) of the Hippocampus (*P<0.05 and **P<0.01 respectively). h–j, % GFAP-positive clasmatodendrocytes were also increased in BCAS-Std group. EE reduced clasmatodendrosis in all subfields (CA1 (h), CA2−3 (i) and CA4 (j)) of the Hippocampus (*P<0.05 and **P<0.01 respectively).

3.5. Positive effects of EE on microglial/macrophage proliferation

There was profound Iba-1 immunostained microglial/macrophage proliferation and activation in the BCAS mice (Fig. 5a). Ramified microglial/ macrophage density was also increased in BCAS in all hippocampal subfields (Fig. 5e–g); a finding replicated by assessing the density of primed/activated microglia/macrophage (> 7 μm) (Fig. 5h–j). In both cases, EE prevented increases in microglial/macrophage numbers in all hippocampal subfields (P<0.01). In the CA1 region, BCAS-std showed higher densities of total Iba-1-positive microglia/ macrophage when compared to BCAS-full (P=0.014), with the CA2−3 and CA4 subfields exhibiting similar trends (Fig. 5b–d). There were no differences, however between groups in any of subfields when microglia/macrophage were stratified into primed/activated and ramified types (Fig. 5e–j).

Brain Research Bulletin 163 (2020) 72–83

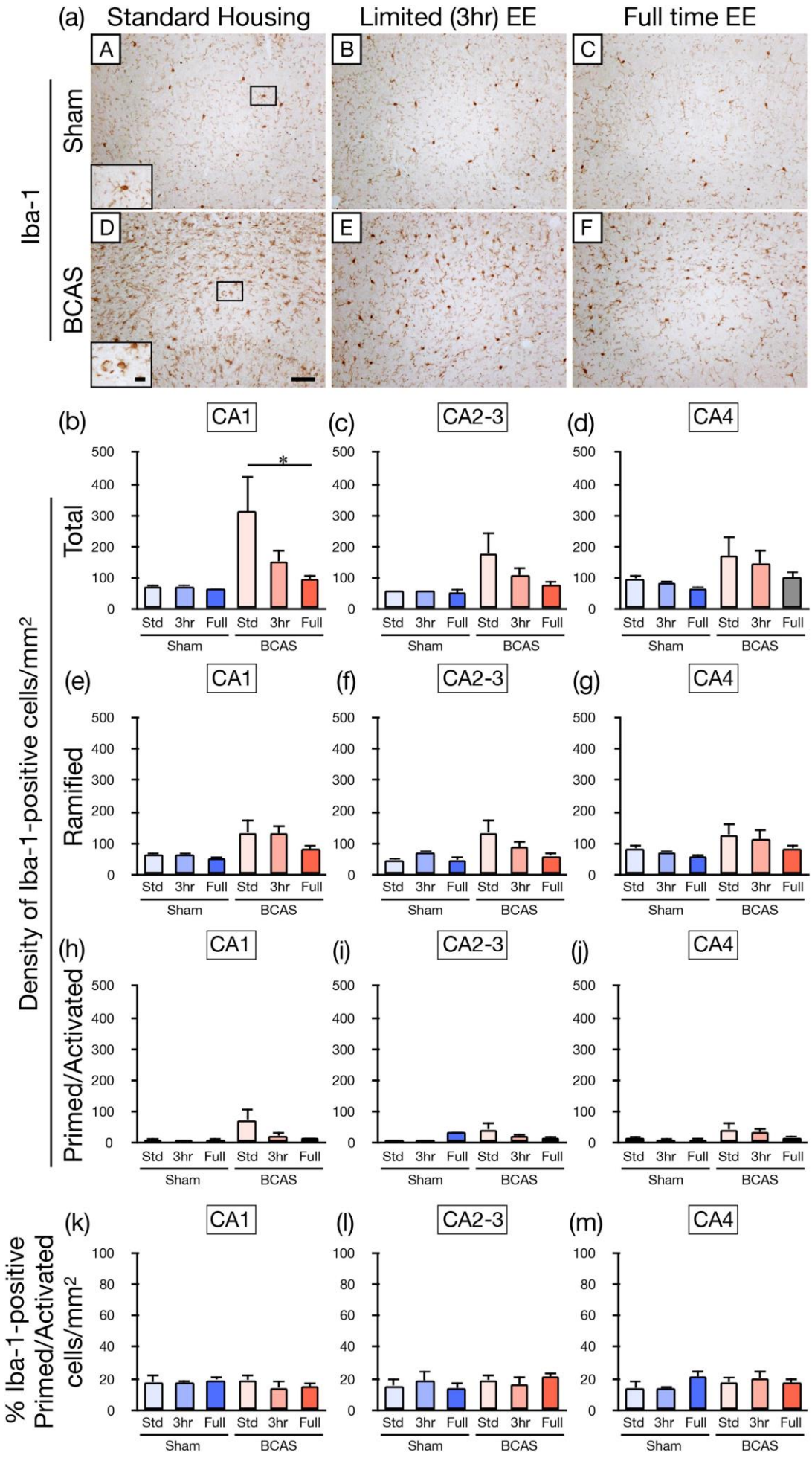

Fig. 5. Assessment of microglial/macrophage activation in the Hippocampus after long-term bilateral common carotid artery stenosis (BCAS).

a(A–F), Representative images of Hippocampus stained with ionised calcium-binding adaptor protein-1 (Iba-1), a marker of microglia/macrophage, in each group. a(A), Sham-Std; a(B), Sham-3 h; a(C), Sham-Full; a(D), BCAS-Std; a(E), BCAS-3 h; a(F), BCAS-Full. a(A and D), Insets showing a normal Iba-1-positive microglia/macrophage in Sham (a(A)) and a primed/activated microglia/macrophage observed in BCAS group (a(D)). Scale bar = 50 µm; Scale bar in insets = 10 µm. b–k, Histograms showing density of total Iba-1-positive microglia/macrophage (b–d), density of Iba-1-positive ramified cells (e–g), density of Iba-1-positive primed/activated cells (h–j), and % Iba-1-positive primed/activated cells (k–m) in CA1 (b, e, h and k), CA2−3 (c, f, i and l) and CA4 (d, g, j and m) subfields of the Hippocampus. b–d, Density of total Iba-1-positive microglia/macrophage was increased in BCAS-Std group in CA1 subregion. EE attenuated microglial/macrophage response in CA1 (b) (*$P < 0.05$). In CA2−3 and CA4 subfields of the Hippocampus, BCAS-Std group showed slightly higher density of total Iba-1-positive microglia/macrophage and attenuation with EE (c and d) ($P<0.10$). e–j, Density of Iba-1-positive ramified cells (e–g) and density of Iba-1-positive primed/activated cells were also slightly higher in all subfields (CA1 (e and h), CA2−3 (f and i) and CA4 (g and j)) of the Hippocampus. These microglial/macrophage responses were partially attenuated by EE ($P<0.10$). k–m, % Iba-1-positive primed/activated cells were not changed amongst all Sham and BCAS groups ($P>0.05$).

3.6. Decreased BDNF expression and acceleration in regenerating neurons

Total hippocampal BDNF levels were decreased in the BCAS-std group compared the sham animals ($P<0.05$). EE did not completely prevent reductions in BDNF levels in either the BCAS-full or BCASlimited compared to the sham groups ($P = 0.089$ vs BCAS-std) (Fig. 6a). We used EdU staining method to demonstrate whether EE influenced the status of proliferating cells within the hippocampus. While no other hippocampal sub-region exhibited any positive staining, we found that there were a significant number of EdU+cells in the dentate gyrus (DG) between the BCAS and sham animals. Furthermore, number of EdU + cells increased in BCAS mice exposed to EE, EdU + cells in the DG were greater in the BCAS-full group compared to sham ($P<0.05$) (Fig. 6c). These observations were also consistent using Ki67 as marker of proliferating cells (Fig. 6b).

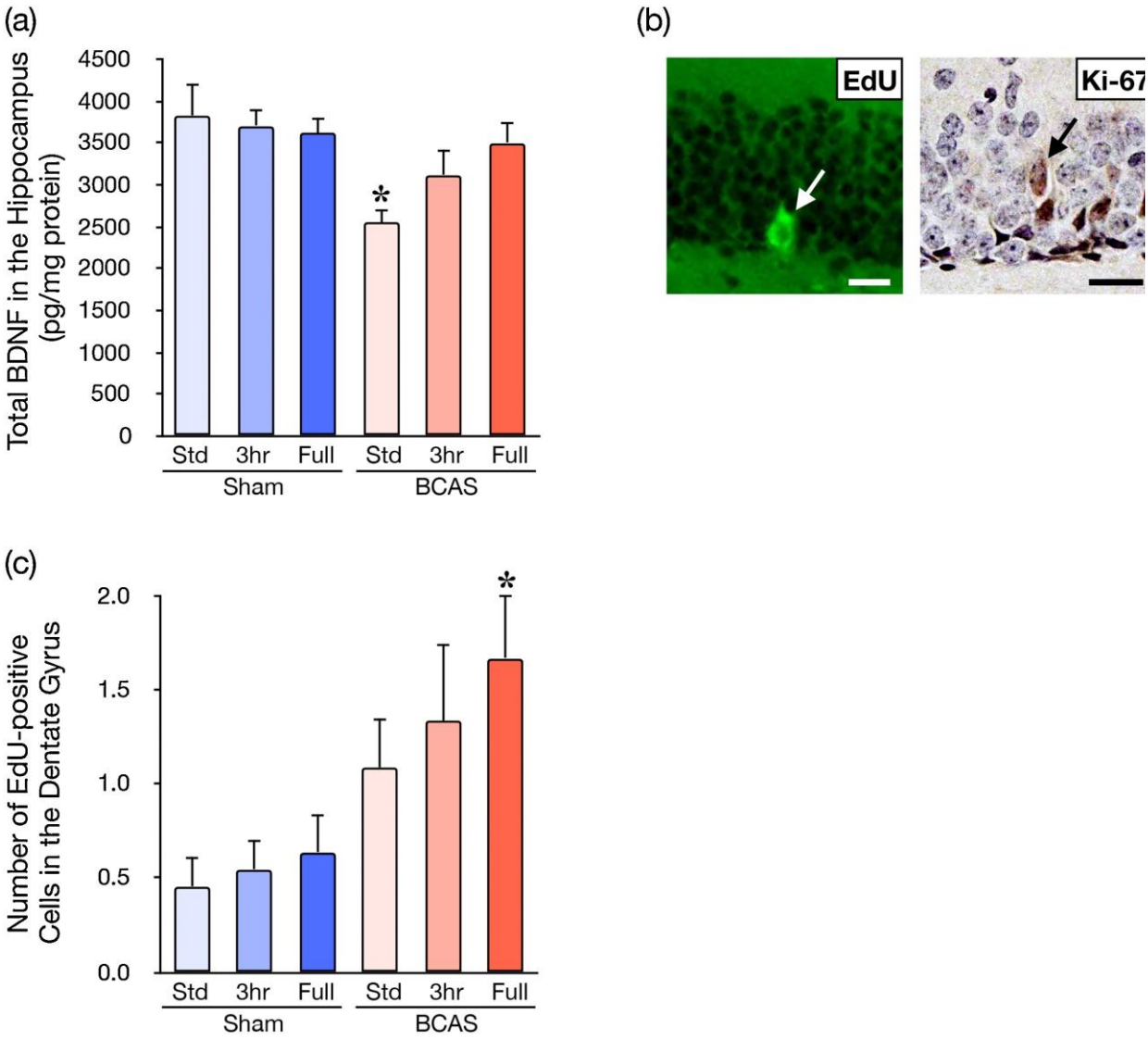

Fig. 6. BDNF expression and assessment of regenerating neurons in the Hippocampus after bilateral common carotid artery stenosis (BCAS).

a, Histogram showing total amount of brain derived neurotrophic factor (BDNF) in the Hippocampus analysed by enzyme-linked immunosorbent assay (ELISA) in each group. Long-term BCAS caused reduction of total BDNF expression in the Hippocampus compared with all Sham groups (*P<0.05). Amongst BCAS subgroups, EE induced more BDNF expression after BCAS (P = 0.09, BCASStd vs BCAS-Full). b, Images show EDU + and Ki67+ granule cells in the same region of DG. c, Histogram showing number of EdU (5- ethynyl-2'-deoxyuridine)-positive neurons (regenerating neurons) in the dentate gyrus (DG) in each group. BCAS induced neuroregeneration in the DG and EE enhanced neuroregeneration after long-term BCAS compared with all Sham groups (*P<0.05).

3.7. Working memory deficits after BCAS

BCAS led to deficits in spatial working memory as represented by lower number of arm entries before first repeat (NABFR) scores. (Fig. 7a–c). The overall differences between sham and BCAS were evident within each BCAS group exhibiting significantly lower NABFR scores against all three sham groups (Fig. 7b). This effect was more evident in the second period of testing sessions (sessions 11–20), which showed NABFR scores for the sham groups increased whereas those in BCAS groups stayed relatively the same (Fig. 7c). It should be noted that the NABFR scores there were differences between

BCAS-3 h and BCAS-full groups across the two halves of sessions. In both cases, scores in the BCAS-3 h group increased over time, whereas in the BCAS-full group they decreased (Fig. 7c). Interestingly, there was strong correlation (p = 0.031) between NABFR scores and number of CA1 neurons, suggesting that the neuronal loss seen in the CA1 region has an important role influencing NABFR scores in the BCAS mice (Fig. 7d).

(a)

Number of arm entries before first repeat (NABFR)	1	2	3	4	5	6	7	8	9
NABFR score (Probability %)	**-11.93** (11.11)	**-3.29** (19.75)	**0.00** (23.05)	**2.56** (20.48)	**8.82** (14.23)	**15.46** (7.59)	**20.09** (2.95)	**22.30** (0.75)	**22.95** (0.09)

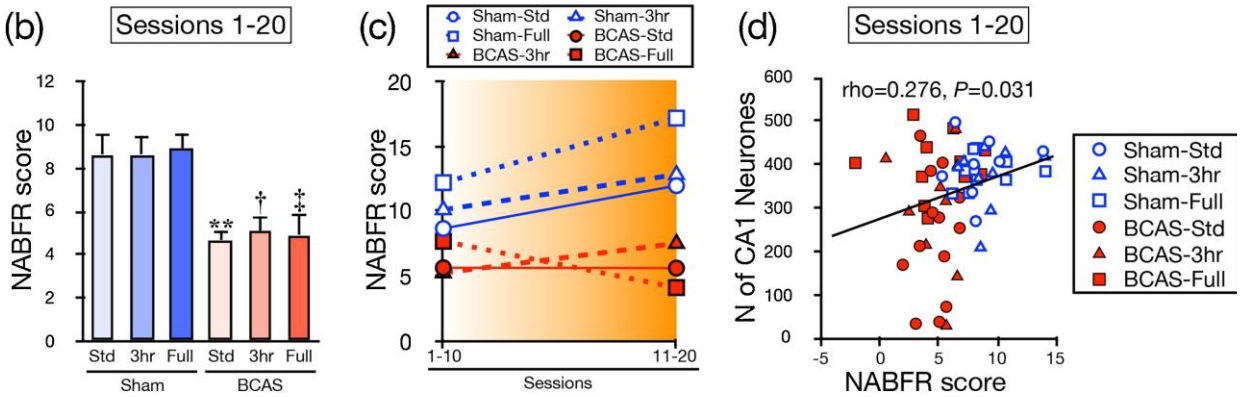

Fig. 7. Assessment of working memory deficit after long-term bilateral common carotid artery stenosis (BCAS).

a, Number of arm entries before first repeat (NABFR) scores and probability of each number of arm entries before first repeat (%). NABFR scores were defined based upon the difference in % compared with the most probable number of NABFR. Three arm entries before first repeat is the most probable (23.05 %) NABFR. Its NABFR score was defined as '0.00' (null). b, Histogram showing NABFR score averaged from sessions 1–20. Average NABFR score of all the sessions 1–20 was lower in BCAS subgroups (**P<0.01; †P<0.05; ‡P<0.05 compared with all Sham groups). c, Graph showing changes in average NABFR score between the former half (sessions 1–10) and the latter half (11–20) in each animal group. All sham groups improved scores towards the end of the session, whereas BCAS remained in low scores with less improvement. d, NABFR score averaged from all sessions 1–20 positively correlated with total number of neurons in CA1 of the Hippocampus (Spearman's rho= 0.28, P = 0.031).

4. Discussion

We report on the favourable effects of EE specifically on hippocampal damage in the BCAS mouse model. We found that chronic cerebral hypoperfusion induced by bilateral common carotid artery stenosis (BCAS) caused neuronal loss in the hippocampus, astrogliosis, clasmatodendrosis (increased number of clasmatodendrocytes) and microglial/macrophage proliferation/activation in the hippocampus. This study provides strong evidence to support the notion that limited EE could suppress brain hypoperfusion-induced neuronal and glial damage in the hippocampus in VCI and possibly VaD patients.

Additionally, it was shown to particularly improve outcomes in the CA1 region, shown to be the most affected in the hippocampus.

Stroke is related to a two to nine fold increase in risk of dementia (Kokmen et al., 1996) with 64 % of persons who experience a stroke having some degree of cognitive impairment (Hachinski et al., 2006). A systematic review including nine studies showed that increased physical activity after stroke improves cognitive performance (Cumming et al., 2012). Our previous study showed that in the whole brain BCASstd induced stroke injury in 100 % of the mice whilst the incidence of infarcts was reduced by 40 % in the mice with limited exposure to EE (BCAS-3 h) and by 33.3 % in the BCAS-full mice. The BCAS-3 h group also tended to have smaller infarcts compared with BCAS-std and BCAS-full groups (Hase et al., 2019). This study showed similarly that environmental enrichment lead to a decrease in lesion size following stroke, as well as resulting in a complete elimination of lesions in the dentate gyrus. This suggests that physical exercise after stroke could reduce the pathological load on the hippocampus leading to improved cognitive outcomes, as has been seen in studies looking at exercise training for cardiovascular disease management (Mijajlovic et al., 2017).

BCAS-induced chronic cerebral hypoperfusion causes selective damage to the CA1 hippocampal subfield, as evidenced by a decrease in CA1 neuronal counts at 3 levels in both H&E and NeuN analysed sections. In contrast, the CA3 showed a greater resistance to hypoperfusion induced pathology, with only mild reductions in neuronal numbers. Notably, BCAS-induced cerebral hypoperfusion causes extensive neuronal loss in the CA1 hippocampal subfield, whilst the CA3 and CA4 display a relative resistance to hypoperfusion. This is in accordance with previous studies showing that brain regions with a high baseline metabolic activity such as the CA1 are extremely susceptible to alterations in cerebral blood flow (Payabvash et al., 2011). This finding is mirrored in longer term BCAS models in which chronic cerebral hypoperfusion results in neuronal loss and atrophy in the hippocampal CA1 subregion, in addition to a relative sparing of other hippocampal regions (Nishio et al., 2010). Parallel to this, clinical findings have shown that patients with AD and SIVD display a similar pattern of neuronal degeneration and atrophy of the CA1 hippocampal sub-region, with concomitant reductions in regional cerebral blood flow to limbic structures including the hippocampus (Kril et al., 2002). Furthermore, recent evidence based on 11C-Pittsburg compound-B positron emission tomography, identified that dementia patients with pure subcortical vascular based pathology display subtle changes in hippocampal volume and shape which further bolsters the translational relevance of these findings (Kim et al., 2015). In this study, we demonstrated that CA1 neuronal loss was strongly related to stroke volumes in the hippocampus, suggesting that vascular brain injury induced by long-term BCAS is directly responsible for some neuronal loss in CA1 region but we were also careful to assess neuronal counts in sections devoid of any infarction.

It has long been established that the CA1 is preferentially affected by neurodegenerative pathologies, such as ischaemia and hypoxia (Bartsch et al., 2015; Bothe et al., 1986; Nikonenko et al., 2009). The basis of this heterogeneous susceptibility to cellular damage is poorly understood but may include glutamate mediated neuronal excitotoxicity, oxidative stress or inflammatory changes (Bartsch et al., 2015). High intrinsic oxidative stress may underlie the regional vulnerability of the CA1 to hypoperfusion (Mattiasson et al., 2003). Cerebral hypoperfusion causes an imbalance between the production and detoxification of reactive oxygen species (ROS), leading to the oxidative modification of proteins and lipids, which may be an initiating event in neuronal death (Wang and Michaelis, 2010). This may also explain the relative resistance of the CA3 to hypoperfusion-induced death, although the CA1 and CA3 are adjacent structures composed of morphologically similar neurons. Experimental studies measuring superoxide formation have shown that CA1 neurons contain significantly

higher levels of superoxide anion than CA3 neurons (Wang et al., 2005). Furthermore, micro-array analysis has shown that CA1 neurons express higher levels of anti-oxidant and ROS producing genes than other hippocampal regions (Wang et al., 2009).

In addition, we found that CA1 has more clasmatodendrocytes (Hase et al., 2018) than all the other subfields, indicating the vulnerability of that region. This complements other studies that show the liability of CA1. Neurons are thought to be the most vulnerable to ischaemia, with astrocytes showing some resistance although this is reduced when placed in particularly acidic conditions (Xu et al., 2001). When the brain experiences cerebral ischaemia, the metabolic activity is suppressed and the structure is damaged. This leads to secondary activation, such as glutamate-mediated excitotoxicity, and consequently cell death (Giffard and Swanson, 2005). This excitotoxicity is partly due to astrocyte function impairment – there is overstimulation of post-synaptic glutamate receptors because there is reduced uptake of glutamate from the synaptic cleft (Alvarez-Maubecin et al., 2000). The heterotypic coupling from astrocytes means there is a connection with neuronal synapses – if this is lost, the protective role of astrocytes is decreased, leading to further damage (Hase et al., 2017). The CA1 region shows a quick reduction in glutamate uptake compared to DG astrocytes – this could explain the relative resistance of DG astrocytes compared to CA1 (Ouyang et al., 2007). The damage to CA1 astrocytes precedes the neuronal death, suggesting the cell death is secondary to astrocyte dysfunction.

In the present study, EdU positive cells were observed in both BCAS and sham animals. The number of EdU positive cells in the BCAS full group was significantly higher than that of the BCAS standard group, which would appear to support the notion that EE stimulates neurogenesis (Speisman et al., 2013). However, experimental models have also shown that chronic cerebral hypoperfusion in itself can stimulate neurogenesis (Sivilia et al., 2008), which is corroborated by the increased number of EdU positive cells in BCAS groups compared to sham. Despite the ambiguity of the exact mechanisms of cellular proliferation in the DG, it is likely multifactorial encompassing both the ability of neuronal pathology to increase cellular proliferation and EE to stimulate neurogenesis and promote cell survival.

The response of microglia/macrophage might be dependent on different degrees of activation and may be detrimental. Tumour necrosis factor-alpha (TNF-α) produced by activated microglia/macrophage plays a critical role in the induction of neuronal death in Alzheimer's disease (Bhaskar et al., 2014). Additionally, human AD cases with increased colony-stimulating factor 1 receptor (CSF1R) expression exhibited increased proliferation of microglia and inhibition of CSF1R decreased microglial proliferation in a mice model of AD (Olmos-Alonso et al., 2016). Earlier studies have suggested that overproduction of cytotoxic factors such as proteases (i.e. matrix metalloproteinase- 2 (MMP-2)), reactive oxygen species and pro-inflammatory cytokines (Planas et al., 2001; Weinstein et al., 2010; Zielasek and Hartung, 1996) that promote neurotoxicity and neuronal damage can be caused by chronic over-activation of microglia results. Chronic cerebral hypoperfusion induces MMP-2, which has roles in BBB disruption, glial activation, and WM lesions after chronic cerebral hypoperfusion (Nakaji et al., 2006), in microglia (Ihara et al., 2001).

A 9-arm radial maze, with raised bridge sections leading to open arms, was used to assess working memory. The results show the deficit seen in BCAS mice ameliorated in those exposed to EE, as seen in our previous studies (Ennaceur et al., 2008; Hase et al., 2017; Hase et al., 2019). Activation of the fronto-subcortical circuits could enhance cognitive function and prevent cognitive decline after cerebral hypoperfusion, which may have been effectively achieved in the limited enrichment group, due to the repeated and time-constrained introduction of the enrichment. The higher scores seen in both indices by the BCAS-3 h group were present more clearly in the later set of sessions (11–20) that are explained by the fact that early sessions trigger more emotional responses

induced by novelty and unfamiliarity of the open spaces within the maze. These responses subside over time after repeated exposures (Ennaceur et al., 2008). This phenomenon would also explain why BCAS-full animals scored high in the early sessions and then regressed. It would seem disruption of the fronto-subcortical circuits lead to similar symptoms of “disinhibition” evident in patients with VaD and frontal lobe dysfunction, overcoming the anxiety response normally present in early trials (Ennaceur et al., 2006).

We also suggest the higher mortality in a proportion of the BCASfull group is explained by dehydration and acute renal failure possibly due to increased overriding physical activity promoted by full-time exposure to EE. Although EE exposes the animals to a number of different features including physical exercise and social interactions, we noted fivefold greater wheel rotations in the BCAS-full subgroup compared to BCAS-3 h, Sham-3 h and Sham-full subgroups (data not shown).

One of the few limitations of our study is that we assessed BCAS-induced hippocampal pathologies at a single time point, 4 months after surgery. Data obtained from several time points, while cumbersome would be useful to understand the temporal profile of hippocampal responses to ischaemic insults as well as to determine the least required duration of EE to ameliorate hippocampal cerebrovascular changes after BCAS. Another limitation is that we only set limited exposure to EE regime at 3 h a day. Testing other durations of limited EE will elucidate the optimal effects of limited exposure to EE against cerebrovascular pathologies in the hippocampus over a period of time, as little is known of EE for the most effective way to modify these pathologies.

5. Conclusions

In summary, long-term chronic cerebral hypoperfusion induced by BCAS could be considered as a relevant VaD model, as it produced neuropathological changes in the hippocampus similar to those seen in VaD patients. This study also demonstrated that EE effectively reduced strokes, protected neurones and preserved neurovascular units and likely BBB integrity, and suppressed detrimental glial activation/proliferation after chronic cerebral hypoperfusion-induced vascular insults in the hippocampus, resultant in amelioration of cognitive decline. EE, and even combination of EE and poly pharmacological approaches would be safe and effective interventional strategies for cerebrovascular disorders which lead to dementia.

Funding

Our study was supported by a grant (ARUK PG2013-22) from Alzheimer’s Research UK. Y.H. was supported by SENSHIN Medical Research Foundation, Osaka, Japan and The Great Britain Sasakawa Foundation, London, UK.

Credit authorship contribution statement

William Stevenson: Methodology, Validation, Formal analysis, Writing - original draft. **Yoshiki Hase:** Conceptualization, Methodology, Validation, Formal analysis, Writing - review & editing. **Elle Wilson:** Validation, Formal analysis. **Annabel Hollins:** Validation, Formal analysis. **Mai Hase:** Methodology, Validation, Formal analysis. **Abdel Ennaceur:** Methodology, Resources, Validation, Formal analysis, Writing - review & editing. **Lucy Craggs:** Methodology, Validation, Formal analysis. **Masafumi Ihara:** Methodology, Validation, Formal analysis, Writing - review & editing. **Karen Horsburgh:** Conceptualization, Methodology, Validation, Formal analysis, Writing - review & editing. **Raj N. Kalaria:** Conceptualization, Methodology, Validation, Formal analysis, Writing - review & editing, Supervision, Project administration, Funding acquisition.

Declaration of Competing Interest

The authors declared no potential conflicts of interest with respect to the research, authorship and/or publication of this article.

Acknowledgements

We specially thank Neil Hamilton and Sandra Hogg for excellent technical assistance with respect to the daily care of mice and animal husbandry. We thank Mary Johnson and Lynn Ramsey (Newcastle University) for excellent technical assistance in processing brain tissue. We are grateful to Hana Matušková (Prague, Czech Republic) for assisting us with the BDNF ELISA and taking some of the images during her summer studentship in 2016.

Appendix A. Supplementary data

Supplementary material related to this article can be found, in the online version, at doi: https://doi.org/10.1016/j.brainresbull.2020.07.014.

References

Alvarez-Maubecin, V., Garcia-Hernandez, F., Williams, J.T., Van Bockstaele, E.J., 2000. Functional coupling between neurons and glia. J. Neurosci. 20, 4091–4098.

Bartsch, T., Dohring, J., Reuter, S., Finke, C., Rohr, A., Brauer, H., Deuschl, G., Jansen, O., 2015. Selective neuronal vulnerability of human hippocampal CA1 neurons: lesion evolution, temporal course, and pattern of hippocampal damage in diffusionweighted MR imaging. J. Cereb. Blood Flow Metab. 35, 1836–1845.

Bayat, M., Sharifi, M.D., Haghani, M., Shabani, M., 2015. Enriched environment improves synaptic plasticity and cognitive deficiency in chronic cerebral hypoperfused rats. Brain Res. Bull. 119, 34–40.

Bhaskar, K., Maphis, N., Xu, G., Varvel, N.H., Kokiko-Cochran, O.N., Weick, J.P., Staugaitis, S.M., Cardona, A., Ransohoff, R.M., Herrup, K., Lamb, B.T., 2014. Microglial derived tumor necrosis factor-alpha drives Alzheimer's disease-related neuronal cell cycle events. Neurobiol. Dis. 62, 273–285.

Bink, D.I., Ritz, K., Aronica, E., van der Weerd, L., Daemen, M.J., 2013. Mouse models to study the effect of cardiovascular risk factors on brain structure and cognition. J. Cereb. Blood Flow Metab. 33, 1666–1684.

Bothe, H.W., Bosma, H.J., Hofer, H., Hossmann, K.A., Angermeier, W.F., 1986. Selective vulnerability of hippocampus and disturbances of memory storage after mild unilateral ischemia of gerbil brain. Stroke 17, 1160–1163.

Cechetti, F., Worm, P.V., Lovatel, G., Moyses, F., Siqueira, I.R., Netto, C.A., 2012. Environmental enrichment prevents behavioral deficits and oxidative stress caused by chronic cerebral hypoperfusion in the rat. Life Sci. 91, 29–36.

Chen, A., Akinyemi, R.O., Hase, Y., Firbank, M.J., Ndung'u, M.N., Foster, V., Craggs, L.J., Washida, K., Okamoto, Y., Thomas, A.J., Polvikoski, T.M., Allan, L.M., Oakley, A.E., O'Brien, J.T., Horsburgh, K., Ihara, M., Kalaria, R.N., 2016. Frontal white matter hyperintensities, clasmatodendrosis and gliovascular abnormalities in ageing and post-stroke dementia. Brain 139, 242–258.

Cumming, T.B., Tyedin, K., Churilov, L., Morris, M.E., Bernhardt, J., 2012. The effect of physical activity on cognitive function after stroke: a systematic review. Int. Psychogeriatr. 24, 557–567.

de Groot, J.C., de Leeuw, F.E., Oudkerk, M., van Gijn, J., Hofman, A., Jolles, J., Breteler, M.M., 2000. Cerebral white matter lesions and cognitive function: the Rotterdam scan study. Ann. Neurol. 47, 145–151.

den Heijer, T., Geerlings, M.I., Hoebeek, F.E., Hofman, A., Koudstaal, P.J., Breteler, M.M., 2006. Use of hippocampal and amygdalar volumes on magnetic resonance imaging to predict dementia in cognitively intact elderly people. Arch. Gen. Psychiatry 63, 57–62.

Ennaceur, A., 2011. Omission of the habituation procedure in the acquisition of a working memory task - evidence from Balb/c, C57/BL6J, and CD-1 mice. Behav. Brain Res. 223, 203–210.

Ennaceur, A., Michalikova, S., van Rensburg, R., Chazot, P.L., 2006. Models of anxiety: responses of mice to novelty and open spaces in a 3D maze. Behav. Brain Res. 174, 9–38.

Ennaceur, A., Michalikova, S., van Rensburg, R., Chazot, P.L., 2008. Detailed analysis of the behavior and memory performance of middle-aged male and female CD-1 mice in a 3D maze. Behav. Brain Res. 187, 312–326.

Ennaceur, A., Michalikova, S., van Rensburg, R., Chazot, P.L., 2011. MK-801 increases the baseline level of anxiety in mice introduced to a spatial memory task without prior habituation. Neuropharmacology 61, 981–991.

Fischer, A., 2016. Environmental enrichment as a method to improve cognitive function. What can we learn from animal models? Neuroimage 131, 42–47.

Giffard, R.G., Swanson, R.A., 2005. Ischemia-induced programmed cell death in astrocytes. Glia 50, 299–306.

Gomez-Nicola, D., Fransen, N.L., Suzzi, S., Perry, V.H., 2013. Regulation of microglial proliferation during chronic neurodegeneration. J. Neurosci. 33, 2481–2493.

Grundman, M., Jack, C.R., Petersen, R.C., Kim, H.T., Taylor, C., Datvian, M., Weiner, M.F., DeCarli, C., DeKosky, S.T., van Dyck, C., Darvesh, S., Yaffe, K., Kaye, J., Ferris, S.H., Thomas, R.G., Thal, L.J., Study, t.As.D.C., 2003. Hippocampal volume is associated with memory but not nonmemory cognitive performance in patients with mild cognitive impairment. J. Mol. Neurosci. 20, 241–248.

Grysiewicz, R., Gorelick, P.B., 2012. Key neuroanatomical structures for post-stroke cognitive impairment. Curr. Neurol. Neurosci. Rep. 12, 703–708.

Hachinski, V., Iadecola, C., Petersen, R.C., Breteler, M.M., Nyenhuis, D.L., Black, S.E., Powers, W.J., DeCarli, C., Merino, J.G., Kalaria, R.N., Vinters, H.V., Holtzman, D.M., Rosenberg, G.A., Wallin, A., Dichgans, M., Marler, J.R., Leblanc, G.G., 2006. National Institute of Neurological Disorders and stroke-Canadian stroke network vascular cognitive impairment harmonization standards. Stroke 37, 2220–2241.

Hase, Y., Craggs, L., Hase, M., Stevenson, W., Slade, J., Chen, A., Liang, D., Ennaceur, A., Oakley, A., Ihara, M., Horsburgh, K., Kalaria, R.N., 2018. The effects of environmental enrichment on white matter pathology in a mouse model of chronic cerebral hypoperfusion. J. Cereb. Blood Flow Metab. 38, 151–165.

Hase, Y., Craggs, L., Hase, M., Stevenson, W., Slade, J., Lopez, D., Mehta, R., Chen, A., Liang, D., Oakley, A., Ihara, M., Horsburgh, K., Kalaria, R.N., 2017. Effects of environmental enrichment on white matter glial responses in a mouse model of chronic cerebral hypoperfusion. J. Neuroinflammation 14, 81.

Hase, Y., Polvikoski, T.M., Ihara, M., Hase, M., Zafar, R., Stevenson, W., Allan, L.M., Ennaceur, A., Horsburgh, K., Gallart-Palau, X., Sze, S.K., Kalaria, R.N., 2019. Carotid artery disease in post-stroke survivors and effects of enriched environment on stroke pathology in a mouse model of carotid artery stenosis. Neuropathol. Appl. Neurobiol. 45, 681–697.

Holland, P.R., Searcy, J.L., Salvadores, N., Scullion, G., Chen, G., Lawson, G., Scott, F., Bastin, M.E., Ihara, M., Kalaria, R., Wood, E.R., Smith, C., Wardlaw, J.M., Horsburgh, K., 2015. Gliovascular disruption and cognitive deficits in a mouse model with features of small vessel disease. J. Cereb. Blood Flow Metab. 35, 1005–1014.

Ihara, M., Tomimoto, H., 2011. Lessons from a mouse model characterizing features of vascular cognitive impairment with white matter changes. J. Aging Res. 2011, 978761.
Ihara, M., Tomimoto, H., Kinoshita, M., Oh, J., Noda, M., Wakita, H., Akiguchi, I., Shibasaki, H., 2001. Chronic cerebral hypoperfusion induces MMP-2 but not MMP-9 expression in the microglia and vascular endothelium of white matter. J. Cereb. Blood Flow Metab. 21, 828–834.
Kalaria, R.N., 2016. Neuropathological diagnosis of vascular cognitive impairment and vascular dementia with implications for Alzheimer's disease. Acta Neuropathol. 131, 659–685.
Kim, G.H., Lee, J.H., Seo, S.W., Kim, J.H., Seong, J.K., Ye, B.S., Cho, H., Noh, Y., Kim, H.J., Yoon, C.W., Oh, S.J., Kim, J.S., Choe, Y.S., Lee, K.H., Kim, S.T., Hwang, J.W., Jeong, J.H., Na, D.L., 2015. Hippocampal volume and shape in pure subcortical vascular dementia. Neurobiol. Aging 36, 485–491.
Kokmen, E., Whisnant, J.P., O'Fallon, W.M., Chu, C.P., Beard, C.M., 1996. Dementia after ischemic stroke: a population-based study in Rochester, Minnesota (1960-1984). Neurology 46, 154–159.
Kril, J.J., Patel, S., Harding, A.J., Halliday, G.M., 2002. Patients with vascular dementia due to microvascular pathology have significant hippocampal neuronal loss. J. Neurol. Neurosurg. Psychiatry 72, 747–751.
Lazarov, O., Robinson, J., Tang, Y.P., Hairston, I.S., Korade-Mirnics, Z., Lee, V.M., Hersh, L.B., Sapolsky, R.M., Mirnics, K., Sisodia, S.S., 2005. Environmental enrichment reduces Abeta levels and amyloid deposition in transgenic mice. Cell 120, 701–713.
Madigan, J.B., Wilcock, D.M., Hainsworth, A.H., 2016. Vascular contributions to cognitive impairment and dementia: topical review of animal models. Stroke 47, 1953–1959.
Mattiasson, G., Friberg, H., Hansson, M., Elmer, E., Wieloch, T., 2003. Flow cytometric analysis of mitochondria from CA1 and CA3 regions of rat hippocampus reveals differences in permeability transition pore activation. J. Neurochem. 87, 532–544.
Mijajlovic, M.D., Pavlovic, A., Brainin, M., Heiss, W.D., Quinn, T.J., Ihle-Hansen, H.B., Hermann, D.M., Assayag, E.B., Richard, E., Thiel, A., Kliper, E., Shin, Y.I., Kim, Y.H., Choi, S., Jung, S., Lee, Y.B., Sinanovic, O., Levine, D.A., Schlesinger, I., Mead, G., Milosevic, V., Leys, D., Hagberg, G., Ursin, M.H., Teuschl, Y., Prokopenko, S., Mozheyko, E., Bezdenezhnykh, A., Matz, K., Aleksic, V., Muresanu, D., Korczyn, A.D., Bornstein, N.M., 2017. Post-stroke dementia - a comprehensive review. BMC Med. 15, 11.
Nakaji, K., Ihara, M., Takahashi, C., Itohara, S., Noda, M., Takahashi, R., Tomimoto, H., 2006. Matrix metalloproteinase-2 plays a critical role in the pathogenesis of white matter lesions after chronic cerebral hypoperfusion in rodents. Stroke 37, 2816–2823.
Nikonenko, A.G., Radenovic, L., Andjus, P.R., Skibo, G.G., 2009. Structural features of ischemic damage in the hippocampus. Anat. Rec. (Hoboken) 292, 1914–1921.
Nishio, K., Ihara, M., Yamasaki, N., Kalaria, R.N., Maki, T., Fujita, Y., Ito, H., Oishi, N., Fukuyama, H., Miyakawa, T., Takahashi, R., Tomimoto, H., 2010. A mouse model characterizing features of vascular dementia with hippocampal atrophy. Stroke 41, 1278–1284.
Olmos-Alonso, A., Schetters, S.T., Sri, S., Askew, K., Mancuso, R., Vargas-Caballero, M., Holscher, C., Perry, V.H., Gomez-Nicola, D., 2016. Pharmacological targeting of CSF1R inhibits microglial proliferation and prevents the progression of Alzheimer'slike pathology. Brain 139, 891–907.
Ouyang, Y.B., Voloboueva, L.A., Xu, L.J., Giffard, R.G., 2007. Selective dysfunction of hippocampal CA1 astrocytes contributes to delayed neuronal damage after transient forebrain ischemia. J. Neurosci. 27, 4253–4260.

Pantoni, L., 2010. Cerebral small vessel disease: from pathogenesis and clinical characteristics to therapeutic challenges. Lancet Neurol. 9, 689–701. Payabvash, S., Souza, L.C., Wang, Y., Schaefer, P.W., Furie, K.L., Halpern, E.F., Gonzalez, R.G., Lev, M.H., 2011. Regional ischemic vulnerability of the brain to hypoperfusion: the need for location specific computed tomography perfusion thresholds in acute stroke patients. Stroke 42, 1255–1260.

Planas, A.M., Sole, S., Justicia, C., 2001. Expression and activation of matrix metalloproteinase- 2 and -9 in rat brain after transient focal cerebral ischemia. Neurobiol. Dis. 8, 834–846.

Rawji, K.S., Mishra, M.K., Michaels, N.J., Rivest, S., Stys, P.K., Yong, V.W., 2016. Immunosenescence of microglia and macrophages: impact on the ageing central nervous system. Brain 139, 653–661.

Roman, G.C., Erkinjuntti, T., Wallin, A., Pantoni, L., Chui, H.C., 2002. Subcortical ischaemic vascular dementia. Lancet Neurol. 1, 426–436.

Shibata, M., Ohtani, R., Ihara, M., Tomimoto, H., 2004. White matter lesions and glial activation in a novel mouse model of chronic cerebral hypoperfusion. Stroke 35, 2598–2603.

Sivilia, S., Giuliani, A., Del Vecchio, G., Giardino, L., Calza, L., 2008. Age-dependent impairment of hippocampal neurogenesis in chronic cerebral hypoperfusion. Neuropathol. Appl. Neurobiol. 34, 52–61.

Speisman, R.B., Kumar, A., Rani, A., Pastoriza, J.M., Severance, J.E., Foster, T.C., Ormerod, B.K., 2013. Environmental enrichment restores neurogenesis and rapid acquisition in aged rats. Neurobiol. Aging 34, 263–274.

Sun, H., Zhang, J., Zhang, L., Liu, H., Zhu, H., Yang, Y., 2010. Environmental enrichment influences BDNF and NR1 levels in the hippocampus and restores cognitive impairment in chronic cerebral hypoperfused rats. Curr. Neurovasc. Res. 7, 268–280.

Tullberg, M., Fletcher, E., DeCarli, C., Mungas, D., Reed, B.R., Harvey, D.J., Weiner, M.W., Chui, H.C., Jagust, W.J., 2004. White matter lesions impair frontal lobe function regardless of their location. Neurology 63, 246–253.

Wang, X., Michaelis, E.K., 2010. Selective neuronal vulnerability to oxidative stress in the brain. Front. Aging Neurosci. 2, 12.

Wang, X., Pal, R., Chen, X.W., Limpeanchob, N., Kumar, K.N., Michaelis, E.K., 2005. High intrinsic oxidative stress may underlie selective vulnerability of the hippocampal CA1 region. Brain Res. Mol. Brain Res. 140, 120–126.

Wang, X., Zaidi, A., Pal, R., Garrett, A.S., Braceras, R., Chen, X.W., Michaelis, M.L., Michaelis, E.K., 2009. Genomic and biochemical approaches in the discovery of mechanisms for selective neuronal vulnerability to oxidative stress. BMC Neurosci. 10, 12.

Weinstein, J.R., Koerner, I.P., Moller, T., 2010. Microglia in ischemic brain injury. Future Neurol. 5, 227–246.

Wu, W., Shao, J., Lu, H., Xu, J., Zhu, A., Fang, W., Hui, G., 2014. Guard of delinquency? A role of microglia in inflammatory neurodegenerative diseases of the CNS. Cell Biochem. Biophys. 70, 1–8.

Xu, L., Sapolsky, R.M., Giffard, R.G., 2001. Differential sensitivity of murine astrocytes and neurons from different brain regions to injury. Exp. Neurol. 169, 416–424.

Zarow, C., Vinters, H.V., Ellis, W.G., Weiner, M.W., Mungas, D., White, L., Chui, H.C., 2005. Correlates of hippocampal neuron number in Alzheimer's disease and ischemic vascular dementia. Ann. Neurol. 57, 896–903.

Zielasek, J., Hartung, H.P., 1996. Molecular mechanisms of microglial activation. Adv. Neuroimmunol. 6 (2). https://doi.org/10.1016/0960-5428(96)00017-4.